Reusable granulated silica pillared clay for wastewater treatment, selective for adsorption of Ni(II)

Seyedmehdi Sharifian [a], Neda Asasian-Kolur [b], Hanieh Najafi [c], Bahram Haddadi [b], Christian Jordan [b,*], Michael Harasek [b]

[a] School of Chemical Engineering, Purdue University, West Lafayette, IN, 47907, United States
[b] Technische Universität Wien, Institute of Chemical, Environmental and Bioscience Engineering, Getreidemarkt 9/166, A-1060, Vienna, Austria
[c] Fouman Faculty of Engineering, College of Engineering, University of Tehran, P. O. Box 43515-1155, Fouman, 43516-66456, Iran

ARTICLE INFO

ABSTRACT

The article presents a study on the suitability of silica pillared clay (SPC) encapsulated with biopolymers, such as alginate, chitosan, or a combination of both, for the adsorption of Ni(II) from aqueous solutions. In the current age of stringent environmental regulations, there is an urgent requirement to identify novel sorbents that can be readily commercialized and employed in large-scale systems to efficiently remove and recover metal compounds from wastewater. Therefore, the study aimed to encapsulate powdered silica pillared clay to produce stable granules via a modified solution casting method, which was confirmed through various characterization studies (FESEM, XRF, XRD, BET, and FTIR). The study found that ALG-SPC showed the best adsorption capacity, owing to its relatively high specific surface area and the negative charge of the alginate. In contrast, encapsulation with chitosan resulted in poor performance due to a significant reduction in porosity. The study also investigated the behaviour of ALG-SPC in a binary solution containing both Ni(II) and Cr(VI) and found that it exhibited selectivity for Ni(II) over Cr(VI). The presence of Cr(VI) did not negatively affect Ni(II) adsorption; in contrast, Ni(II) helped to Cr(VI) adsorption under a limited pH range. The study also conducted adsorption mechanism, kinetic, and equilibrium modelling. Recovery of adsorbed Ni(II) from saturated ALG-SPC was most effective in acidic solutions in comparison with electrolyte solution and methanol. The study's findings have important implications for the development of effective and selective adsorbents for heavy metal removal and recovery from wastewater.

1. Introduction

The growth of the world's population and the development of technology and electrical devices have led to an increase in the production of metal-bearing wastes. However, the toxicity and adverse effects of heavy metals on living organisms are one of the world's greatest challenges. Industrial and municipal wastewater often contains various species of these metals such as Ni, Cr, Cd, As, and Hg, which are classified as classical pollutants. Exposure to these pollutants can cause a range of physical and mental diseases and even death (Jaishankar et al., 2014).

Wastewater from the electroplating industry is a significant source of Ni in the environment. Various concentrations for Ni in wastewater are reported, ranging from 20 to 200 mg/L (Revathi et al., 2005) to as high as 1000 mg/L in some cases (Wardani et al., 2017). Similarly,

hexavalent chromium, another highly toxic heavy metal, enters surface waters via wastewater from the tanning and electroplating industries (Chitraprabha and Sathyavathi, 2018). The World Health Organization (WHO) has set guideline values of 0.05 mg/L and 0.02 mg/L for total chromium and nickel, respectively (World Health Organization, 2021). In contrast to organic pollutants, metallic pollutants have inherent value derived from their limited natural sources. Therefore, it is essential to treat these effluents not only to remove metals from the environment but also to recover them for further use.

Several techniques are available for treating metal-containing wastewater. However, chemical precipitation is usually more efficient when the initial concentration of metal pollutants is relatively high. Membrane filtration, electrodialysis, and reverse osmosis are expensive processes, while electrochemical treatment generates a large amount of hazardous waste. Adsorption, on the other hand, is a relatively simple

and effective technology for removing and recovering trace metals (Ince and Ince, 2019). The recovery of metal compounds can be more efficient if done through adsorption and enrichment on an adsorbent with high metal selectivity. Adsorption can be performed selectively by using a suitable and specially designed adsorbent.

In addition to the traditional classical adsorbents such as activated carbon and charcoal, various other classes of adsorbents have been proposed for the adsorption of heavy metals. These include natural inorganic, natural organic (biosorbents), and synthetic materials. Natural inorganic adsorbents include clays, minerals, fly ash, zeolites, and other similar materials. Biosorbents are typically made from a variety of biomass materials, including agricultural residues, microorganisms, and biopolymers (Golnaraghi Ghomi et al., 2020). Synthetic adsorbents include nanosized materials and hybrid composites (Pfeifer and Skerget, 2020). Clay is an inexpensive and environmentally friendly natural resource that is known for its potential as an adsorbent due to its inherent but temporary porous structure (Mnasri-Ghnimi and Frini-Srasra, 2019). Pillared clay, a modified type of clay, is produced by exchanging charge-balancing cations in the interstices between clay layers with polymeric (or oligomeric) cationic species. The intercalated precursors then solidify into columns (pillars) after the calcination process, resulting in increased basal spacing and durable porosity that is maintained even after dehydration. Alumina, iron oxide, zirconia, titania, and silica are the primary pillar formers used in the preparation of pillared clay (Najafi et al., 2021b).

Silica Pillared Clays (SPCs) can be considered a new generation of mesoporous silica materials that have a combination of microporosity within the silica wall and an acidic structure derived from the natural structure of clay. In addition to this, SPCs have additional silanol groups formed by the silica pillar agents (Dincer et al., 2020). The synthesis of SPCs is based on the intercalation of smectite clay layers with long-chain organic surfactants, followed by in-situ micelle formation in the presence of water and subsequent condensation of silica around this template. The key parameters that determine the effectiveness of SPC synthesis are the properties of the raw materials (such as clay properties, organic surfactants, and silica source), their ratios (clay/surfactants/silica/solvent), and the calcination temperature (Dincer et al., 2020).

A literature review indicates that most applications of silica-pillared clays concentrate on the homogeneous catalytic oxidation of organic molecules. For example, Yang et al. (2013) synthesized mesoporous iron-incorporated silica-pillared clay and employed it for the catalytic hydroxylation of phenol (Balcı and Tomul, 2023; Wu et al., 2016; Yang et al., 2013). In another study, Balcı and Tomul (2023) used silica-pillared clays supported by iron and titanium incorporated catalysts for catalytic wet peroxide oxidation of phenol (Balcı and Tomul, 2023; Wu et al., 2016; Yang et al., 2013). The few studies that have examined adsorption by these materials have utilized them for the adsorption of organic molecules, such as pharmaceutical pollutants and antibiotics. For instance, granulated silica pillared clay, which is prepared by intercalating a cationic surfactant (CTAB) into the layers of bentonite clay and then granulating with sodium alginate, has been used for the adsorption of levofloxacin and gemifloxacin (Farajfaed et al., 2021). The adsorption of ciprofloxacin and tetracycline in alkaline aqueous media by silica pillared clay (Roca Jalil et al., 2018) and the adsorption of gemifloxacin by Fe-incorporated silica pillared clay (Najafi et al., 2022b) are also worth mentioning.

Furthermore, few studies have reported on the metal adsorption capacity of silica-pillared clays, which highlights the research gap that the authors of this article aim to address. For example, Addy et al. used modified silica pillared clay for the adsorption of heavy metals. They proposed a two-step modification process involving sequential modification with oxides (silica and ferric oxide) and grafting a chelating agent (tetraethoxysilane and ferric nitrate solution) onto the montmorillonite as the expandable clay. The modified organoclay demonstrated the highest adsorption capacity for heavy metal cations, including Cu^{2+}, Ni^{2+}, Cd^{2+}, Zn^{2+}, Fe^{3+}, and Pb^{4+}, even in acidic media (Addy et al.,

2012). Mao et al. also synthesized a titania silica-pillared clay with a highly ordered mesoporous interlayer structure and found it to be a suitable adsorbent for the removal of Cr(VI) from an aqueous system (Mao et al., 2014).

One of the primary challenges of utilizing laboratory-designed adsorbents is their fine particle size, which can pose difficulties in separating them from treated solutions and bed adsorption systems. A literature review has shown that only a few articles have tackled the granulation of adsorbents, especially when considering non-traditional adsorbents. Therefore, the objective of this study is to investigate and propose a modification method that can simultaneously achieve both the granulation and surface chemical modification of the adsorbents, resulting in enhanced stability and adsorption capacity.

The study aims to achieve an adsorbent with improved adsorption affinity and selectivity towards Ni(II) by utilizing two biopolymers, chitosan and alginate, as well as a combination of the two for modification and granulation of silica pillared clay. The investigation involves conducting kinetic and equilibrium adsorption experiments, as well as examining the recovery of Ni from the saturated effective adsorbent. Furthermore, the influence of Cr(VI) on the efficiency of the adsorbent will also be studied.

2. Materials and methods

The raw clay used in this study was locally sourced from Iran and supplied by Mojallali Co. (Isfahan, Iran). All other chemicals were laboratory-grade quality. This section details the synthesis process for the original Silica Pillared Clay (SPC), including granulation with two different biopolymers, and the characterization techniques employed. Next, the experimental design for batch mode adsorption to remove Ni (II) from aqueous solutions, competitive adsorption of Cr(VI), and solvent extraction of Ni(II) is discussed.

2.1. Adsorbent preparation

2.1.1. Silica pillared clay (SPC)

The SPC was prepared based on a previous study (Najafi et al., 2021a) using the following steps: first, the raw clay was acid-washed, then saturated with sodium. Next, a pillaring solution was prepared by slowly adding tetraethyl orthosilicate to a mixture of ethyl hexadecyl dimethyl ammonium bromide in ethanol and water, which was placed in an ultrasonic bath for 1 h and stirred for 1 h. The pillaring solution was dropwise added to the clay suspension and mixed thoroughly. The molar ratio of the materials CEC:surfactant:tetraethyl orthosilicate:ethanol: water was taken as 2400:80:40:3:1. The pH of the prepared gel was then adjusted to 10 by adding 25% ammonia solution. Finally, the gel was subjected to vacuum filtration, washing, and drying.

A schematic representation of these steps can be seen in Fig. 1. Further details of the procedure can be found in Najafi et al.'s previous study (Najafi et al., 2021a).

2.1.2. Encapsulated SPC beads (ALG-SPC, CS-SPC and ALG/CS-SPC)

To prepare ALG-SPC hydrogel beads, a 2% solution of sodium alginate was prepared and stirred for 1 h at 45 °C to ensure complete homogenization. Subsequently, a 10% suspension of SPC was added to the sodium alginate solution in a ratio of 5:1 (SPC/alginate) and stirred for 4 h at room temperature. The resulting mixture was added dropwise to a coagulation solution consisting of a 2% (w/v) calcium chloride solution, using an 18-gauge needle and syringe. The hydrogel granules formed were stored in a refrigerator at 4 °C for 15 h. The beads were then removed from the solution, filtered, washed several times with distilled water, and dried at 65 °C for 18 h (Najafi et al., 2022a). The method for preparing ALG/CS-SPC is relatively similar to ALG-SPC. However, the polyelectrolyte solution was a mixture of a 2% chitosan solution (prepared in a 2% acetic acid solution) added to a 2% sodium alginate solution, with a pH of 5 to dissolve the chitosan. The weight ratio of
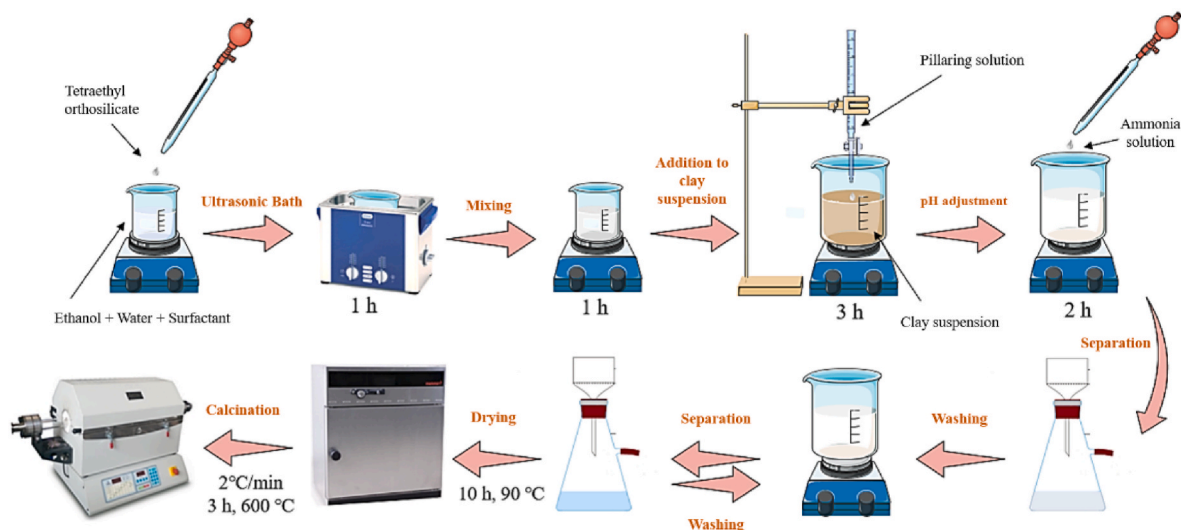
Fig. 1. Schematic representation of the manufacturing process of Silica Pillared Clay (SPC).

SPC/alginate/chitosan was also 5:1:1 (Najafi et al., 2021a).

Similar to the two other sorbents, the chitosan-SPC beads were prepared using a modified solution casting method (Han et al., 2010). In order to ensure comparable conditions for different adsorbents, most parameters were similar to the previous ones. A 2% chitosan solution in a 2% acetic acid solution, a 10% suspension of SPC, and a weight ratio of SPC/chitosan of 5:1 were chosen for the preparation procedure. However, instead of using a calcium chloride solution, a 3% (w/v) NaOH solution was used as the coagulation solution for granulation. The resulting mixture was added dropwise with a syringe and kept for 15 h, followed by a washing procedure to achieve neutral conditions. To maintain the stability of the chitosan beads under acidic conditions, the chitosan chains were cross-linked with glutaraldehyde by contacting the beads with a 0.2% glutaraldehyde solution for 1 h. After separation, the beads were washed several times with distilled water and dried at 65 °C for 18 h.

2.2. Characterization

The raw clay, SPC, ALG-SPC, CS-SPC, and ALG/CS-SPC underwent several characterization analyses, including porosity measurement using BELSORP MINI II and elemental analysis by XRF using a Philips PW1730 wavelength dispersive spectrometer. To investigate the porosity of the samples, they were degassed at 150 °C for 2 h and then subjected to N_2 adsorption-desorption analysis at −196 °C. FESEM micrographs of the raw clay, SPC, and encapsulated samples were obtained using a MIRA3 (TESCAN, Czech Republic) scanning electron microscope. The XRD patterns of the raw clay and encapsulated SPCs were also obtained using a Philips V 1800 spectrometer, with Cu Kα radiation at 40 kV and Ni filtration at 30 mA, and compared with the patterns of pure chitosan and alginate from the literature. FTIR spectra of the samples were recorded using a PerkinElmer spectrum instrument with DTGS detectors between 4000 and 400 cm^{-1}. To investigate the adsorption mechanisms, the ALG-SPC underwent FTIR study before and after Ni(II) adsorption and saturation. The pH_{pzc} of the ALG-SPC was also determined by the pH-drift method (Noh and Schwarz, 1989).

2.3. Batch Ni(II) adsorption and modelling

A series of batch adsorption experiments were performed, including kinetics, equilibrium, and effects of operating parameters (Çeçen and Aktas, 2011). The aim of the first study was to compare the Ni(II) adsorption capacity of various types of pillared clay beads at different pH levels between 2 and 7. The experiment was conducted under the following conditions, with an initial Ni(II) concentration of 50 mg/L, 3 g/L adsorbent dosage, and a shaking speed of 250 rpm. The temperature was maintained at 25 °C, and the contact time was 24 h. Ni(II) stock solutions were prepared using $Ni(NO_3)_2.6H_2O$ dissolved in distilled water. The pH range was selected based on preliminary experiments, and it was found that at pH values above 8, nickel cations began to precipitate.

The most effective adsorbent was further analysed through a series of batch adsorption experiments to investigate the impact of dosage, as well as kinetic and equilibrium studies at the optimal pH. The effect of adsorbent dosage was examined by varying the dosage within a range of 0.5–5 g/L while keeping the initial Ni(II) concentration at 50 mg/L. A series of kinetic experiments was carried out at the best dosage and pH by taking samples at different time intervals ranging from 15 min to 24 h. The equilibrium adsorption experiments were conducted by altering the initial Ni(II) concentration within the range of 30–400 mg/L, and samples were taken after 24 h to ensure that equilibrium was achieved. The concentration of Ni(II) was determined using atomic absorption spectroscopy (Varian AA240) at a wavenumber of 232 nm.

To investigate the selectivity of the ALG-SPC adsorbent for Ni(II), a series of experiments were conducted using solutions containing both Ni (II) and Cr(VI) at different pH values (ranging from 2 to 7). The operating conditions for these experiments were as follows: the initial concentration of both Ni(II) and Cr(VI) ions was 25 mg/L, the adsorbent dosage was 3 g/L, the contact time was 24 h, and the temperature was maintained at room temperature. The Cr(VI)-containing solutions were prepared by dissolving an appropriate amount of K_2CrO_4 salt in distilled water. Cr(VI) concentration was also measured by atomic absorption spectroscopy (Varian AA240) at a wavelength of 537.9 nm.

2.4. Ni(II) desorption experiments

Aqueous solutions of 0.1 M HCl, HNO_3, KCl, and NaCl, as well as pure methanol, were utilized to desorb Ni(II) from nickel-saturated adsorbents. Eluent washing is a common technique used to desorb adsorbed species from different types of adsorbents (Patel, 2021). To prepare the nickel-saturated ALG-SPCs, 50 cm^3 of a nickel-containing solution (50 mg/L and pH = 7) was mixed with the adsorbent (dosage = 3 g/L) and shaken at room temperature and a speed of 250 rpm for 24 h. The adsorbent was then separated from the treated solution, washed, and dried at 90 °C for 2 h before being contacted with the solution to extract the adsorbed metal. For desorption, the saturated and dried adsorbent (0.12 g) was shaken with 25 cm^3 of each of the aforementioned solutions at room temperature for 24 h (250 rpm). The concentration of Ni in the

extraction solutions was determined by atomic absorption spectroscopy. Each adsorption and desorption experiment was conducted at least twice, and the data were obtained with a confidence level of more than 95%.

3. Results and discussion

3.1. Adsorbent characterization

The raw clay used in this study was found to have a high percentage of silica (76 wt%) and alumina (12 wt%) based on Table 1. XRF analysis showed that the main impurities present in the clay were Fe, Mg, Ca, Na, K, Mn, and P oxides. After pillaring with silica, the silica content increased to over 91 wt%, while the other impurities were reduced through the washing and pre-treatment steps. The decrease in the percentage of interlayer cations such as sodium indicates the successful replacement of the cations in the raw clay by the pillaring species. Alginate treatment of the SPC resulted in a slight increase in the CaO content due to the use of a $CaCl_2$ solution for coagulation, while chitosan treatment led to a slight increase in the weight percentage of Na_2O due to the use of a NaOH solution for coagulation.

Table 2 shows a comparison of the porous properties of these adsorbents. The increase in the specific surface area (S_{BET}) of the raw clay can be attributed to the pillaring process, which involves introducing silica pillars between the clay layers. This modification creates permanent mesopores while also resulting in a limited number of micropores in the mesoporous silica pillared clay (SPC). The SPC contains more than 90% mesoporosity, and this modification results in a shift in the average size of mesopores from over 36 Å in the raw clay to less than 29 Å in the SPC.

The granulation process using alginate and chitosan, both individually and in combination, led to a reduction in the porous properties of the samples by obstructing the pores with the binder molecules. However, encapsulation with chitosan resulted in a much higher loss of specific surface area (S_{BET}) compared to alginate. The chitosan-encapsulated SPC (CS-SPC) had an S_{BET} of only about 3 m^2/g and negligible total pore volume. The reduced porosity of the CS-SPC can be confirmed by comparing the appearance of the granules in Fig. 2. Unlike ALG-SPC and ALG/CS-SPC, the CS-SPC had a smaller radius (despite being formed using the same syringe) and did not appear to be porous. The combination of biopolymers in ALG/CS-SPC showed behavior more similar to alginate than chitosan, and the S_{BET} loss was around 24%.

In Fig. 3, the changes in the surface morphology of the clay after pillaring and granulation with alginate and chitosan are illustrated. The smooth internal structure of the raw clay is in contrast to the porous and heterogeneous surface of SPC, ALG-SPC, and CS-SPC, which is clearly visible in Fig. 3. The SPC encapsulated with biopolymers showed a relatively different texture than the powdered SPC. The effect of granulation was apparent in the FESEM images, which showed the transformation of the small clay platelets into spherical particles.

Fig. 4 shows the FTIR spectra of the raw clay, SPC, ALG-SPC, and CS-SPC samples. The raw clay spectrum exhibits a broad peak at 3440 cm^{-1} representing the O-H stretching of Al-OH and Si-OH, and a peak at 3623 cm^{-1} indicating the O-H stretching of adsorbed H_2O molecules. An O-H bending vibration is also observed at 1635 cm^{-1}, while the peak at 1429 cm^{-1} is a CO_3 stretching vibration originating from the calcite structure.

Table 2
Porous properties of the raw clay, original, and granulated SPCs.

Sample	S_{BET} (m²/ g)	V_{TOT} (cm³/ g)	V_{MIC} (cm³/ g)	V_{MES} (cm³/ g)	BJH mesopore size (Å)	Mesoporosity (%)
Raw Clay	40	0.13	0.01	0.13	36.6	~100
SPC	600	1.43	0.22	1.30	28.7	~91
ALG-SPC	497	1.29	0.19	1.17	28.6	~91
CS-SPC	3	0.004	~0	0.004	34.0	~100
ALG/CS-SPC	455	1.20	0.17	1.09	27.0	~91

The Si-O-Si stretching leads to a peak at 1041 cm^{-1}, and the Si-O bending results in small peaks at 800 and 520 cm^{-1} for the raw clay. The peak at 468 cm^{-1} represents the Al-O stretching.

In the spectrum of SPC, peaks at 3435 cm^{-1} and 1639 cm^{-1} represent the O-H stretching and bending vibrations. The absence of the calcite (CO_3 stretching) peak in this spectrum is due to the removal of calcite during pretreatment. The Si-O-Si stretching and Si-O bending resulted in peaks at 1083 and 801 cm^{-1} in this sample. Encapsulation of SPC with pure alginate did not significantly alter the functionalities of SPC, and the main bands of ALG-SPC are attributed to hydroxyl, ether, and carboxyl groups (Daemi and Barikani, 2012).

By analyzing the characteristic FTIR peaks of pure chitosan as described by (Varma and Vasudevan, 2020), and comparing CS-SPC with SPC, it can be inferred that the additional peak at 2876 cm^{-1} in the CS-SPC spectrum is due to CH_2 stretching. The relatively larger peaks observed at 1578 and 1425 cm^{-1} correspond to the vibrational modes of C=O stretching of the amide and C−H side-chain bending –CH_2OH, respectively. The shifts and changes detected in the 800-400 cm^{-1} region can be attributed to out-of-plane N−H bending.

Fig. 5 displays the XRD spectra of several samples within a normal range. Comparing the XRD spectrum of the raw clay with the standard JCPDS maps confirms the presence of montmorillonite (M), quartz (Q), cristobalite (Cr), clinoptilolite (C), and calcite (Ca) as impurities. The spectra of pure alginate (Sayın et al., 2022) and pure chitosan (Aziz et al., 2017) are also shown in this figure, revealing their semicrystalline structures in contrast to the encapsulated SPCs. The XRD pattern of the composites formed by combining SPCs with biopolymers (alginate and chitosan) exhibited peaks representing both materials, with the semi-crystalline structure of the biopolymers masking the crystalline structure of the clay. The modified SPCs showed similar patterns to the biopolymers, while the crystalline structure of the montmorillonite was preserved.

3.2. Batch mode adsorption

The adsorption experiments for Ni(II) were conducted using granular adsorbents that can be easily separated after adsorption. This is in contrast to the powdered adsorbent (SPC), which necessitates time-consuming filtration steps and high-speed centrifugation to separate saturated adsorbents. However, due to the significant difference between the particle size of the granular adsorbents and SPC, and their effective role in the kinetics, equilibrium, and diffusion mechanisms,
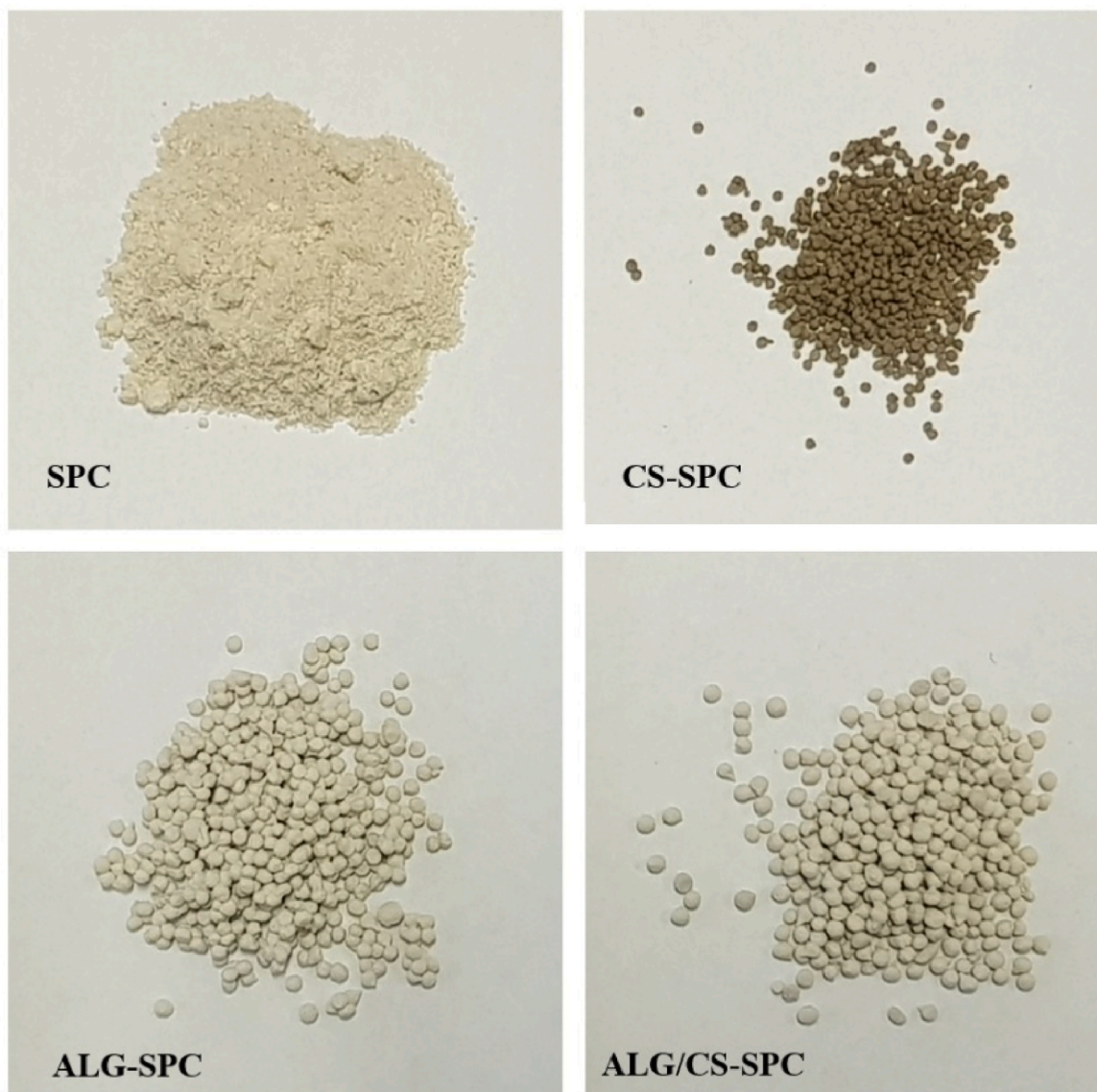
Table 1
Chemical composition (wt%) of raw clay, original and granulated SPCs.

Sample	SiO_2	Al_2O_3	Fe_2O_3	MgO	CaO	Na_2O	K_2O	TiO_2	MnO	P_2O_5
Raw Clay	76.08	12.6	1.74	1.75	4.04	2.02	1.20	0.29	0.06	0.03
SPC	91.36	6.24	0.86	0.61	0.30	0.14	0.34	0.14	<0.01	<0.01
ALG-SPC	91.82	3.54	0.73	0.61	2.93	<0.01	0.24	0.12	<0.01	<0.01
CS-SPC	90.65	5.96	0.88	0.60	0.35	1.14	0.29	0.12	<0.01	<0.01
ALG/CS-SPC	90.85	5.92	0.80	0.60	1.24	0.12	0.31	0.12	<0.01	<0.01

Fig. 2. Appearance of SPC, ALG-SPC, CS-SPC and ALG/CS-SPC.

only the performances of the adsorbents in bead form were compared in this study.

Fig. 6 displays the Ni(II) adsorption capacity of the adsorbents ALG-SPC, CS-SPC, and ALG/CS-SPC as a function of solution pH. It can be observed that ALG-SPC exhibits the highest adsorption capacity for Ni(II), while CS-SPC performs the least effectively. This behaviour can be explained by the surface charge and porosity of the adsorbents. Alginate is a negative biopolymer, and chitosan is a positive biopolymer. The strong electrostatic attraction between the negatively charged alginate and Ni(II) cations is the primary reason for the high efficiency of Ni(II) adsorption by ALG-SPC compared to the other samples. However, chitosan, as a positive biopolymer, weakens the adsorption affinity towards Ni(II) cations. The very small specific surface area and limited porosity of CS-SPC, compared to the other sorbents, is also the main reason for the weak affinity of CS-SPC toward Ni(II). The adsorbent with a combination of chitosan and alginate exhibits intermediate behaviour between ALG-SPC and CS-SPC.

Fig. 6 also demonstrates the positive influence of solution pH on the adsorption capacity of all three types of adsorbents for Ni(II). The primary reason for the lowest capacity at very acidic conditions is the high concentration of H^+ competing with Ni(II) cations for adsorption at the appropriate sites. This indicates the role of electrostatic forces in the adsorption mechanisms. In weakly acidic conditions and near the neutral region, the amount of H^+ cations decreases, allowing for more Ni(II) species to be adsorbed. Additionally, the better performance at higher pH can be attributed to the gradual decrease in the net positive charge on the adsorbent surface, leading to electrostatic attraction between the deprotonated functional groups and the Ni(II) cations. The functional groups with Si-O and COO bonds play a crucial role in this process.

Due to its limited specific surface area and porosity, almost all of the Ni(II) adsorption by CS-SPC occurs through chemical and electrostatic interactions between the adsorbent functional groups and Ni cations. Apart from silanol and carboxyl groups, amine groups ($-NH_3$) in the CS-SPC sample also participate in metal cation adsorption via chelation. Changes in pH also affect the chelation mechanism. Strongly acidic conditions result in protonation of chitosan's amine groups, reducing the number of sites accessible for chelation of Ni(II) cations. Based on the findings, a pH of 7 was selected as the optimal pH within the studied range for further experiments.

Dosage is another crucial parameter that affects the adsorption capacity in a batch process. In this study, the adsorbent dosage was varied
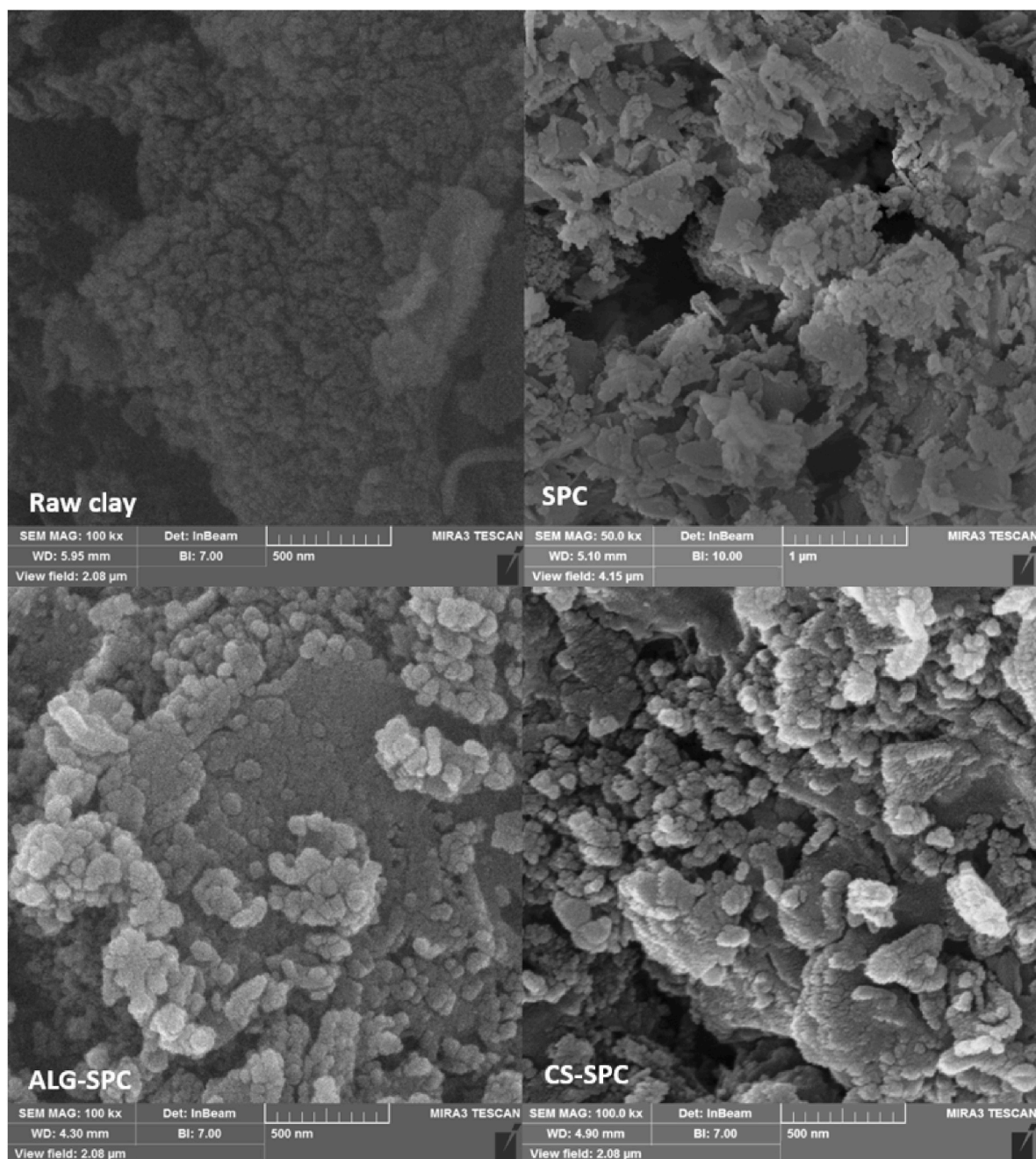
Fig. 3. FESEM micrographs of the raw clay, SPC, ALG-SPC, and CS-SPC.

between 0.5 g/L and 5 g/L, resulting in an increase in adsorption removal from 30% to approximately 70% (Fig. 7). The curve exhibits a plateau shape at high dosages of 4 and 5 g/L, indicating that increasing the dosage beyond these values does not result in a higher adsorption removal. This behaviour is expected, as the adsorption capacity shows an inverse relationship with the adsorbent dosage, which explains the decrease in q as the dosage increases.

According to Fig. 8 (a), which presents experimental kinetic adsorption data up to 48 h, the equilibrium time for the adsorption process is approximately 24 h. The initial slope of the curve indicates a relatively high adsorption rate, with ALG-SPC adsorbing up to 55% of the equilibrium adsorption capacity (about 11 mg/g) of Ni(II) in just 15 min. Two types of kinetic adsorption models were employed to predict and explain the behaviour of the adsorption system: reaction-based kinetic models and diffusion-based models (Sahoo and Prelot, 2020). In

the former, the entire adsorption process, including solute transfer from bulk solution to the surface and mass action, is considered as an integrated process with a rate equation that is similar to a chemical reaction. The pseudo-first order and pseudo-second order models are two of the most common reaction-based kinetic models, presented in their nonlinear form in Table 3. It should be noted that only kinetic data far enough from equilibrium, up to 4 h, were utilized for the kinetic modeling.

Table 3 presents the parameters of the kinetic models and the corresponding statistical correlations, such as the correlation coefficient (R^2), sum of squared errors (SSE), and root mean squared error (RMSE). These values were used to determine the best-fit of the kinetic models. The results show that the pseudo-second order model provides a better fit to the experimental data than the pseudo-first order model. Moreover, the pseudo-second order model predicts an equilibrium adsorption
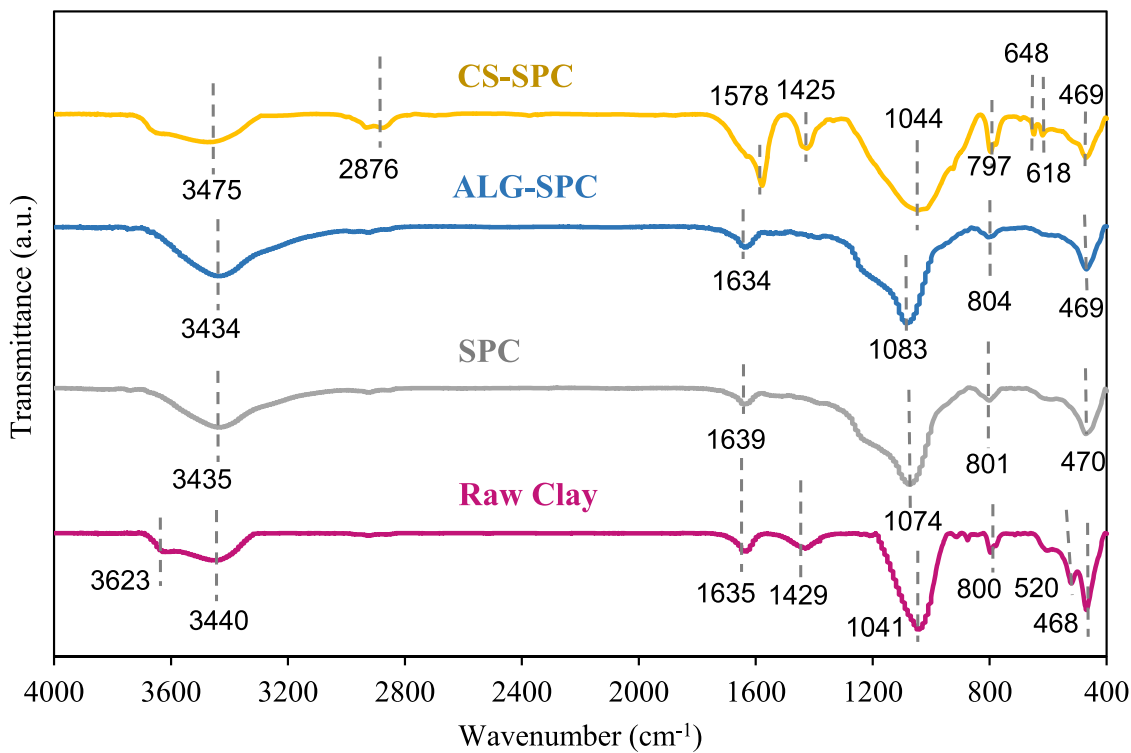
Fig. 4. FTIR spectra of the raw clay, SPC, ALG-SPC, and CS-SPC.
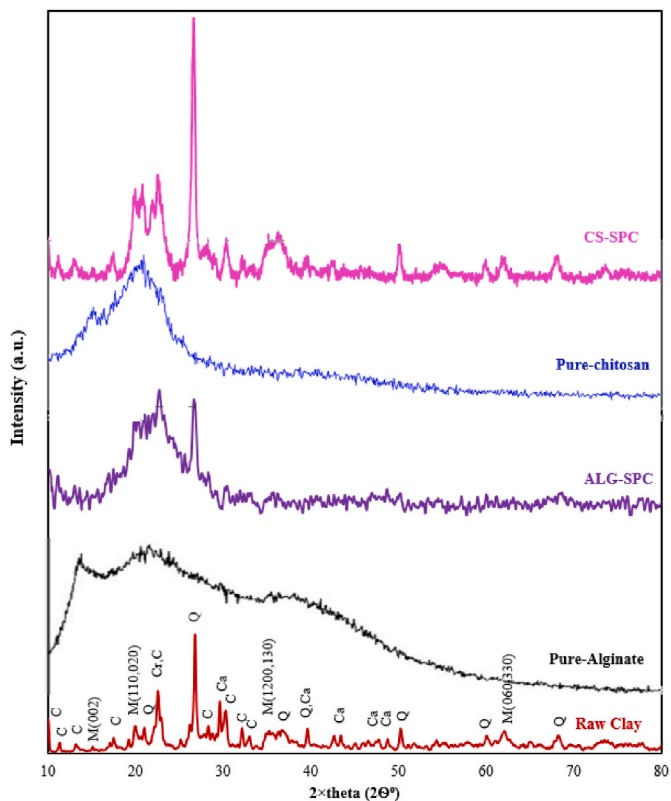

Fig. 5. Normal XRD spectra of the raw clay compared to the pure biopolymers and the SPCs encapsulated with biopolymers. (Pure alginate from (Sayın et al., 2022) and chitosan (Aziz et al., 2017)) (Montmorillonite (M), quartz (Q), cristobalite (Cr), clinoptilolite (C), and calcite (Ca)).
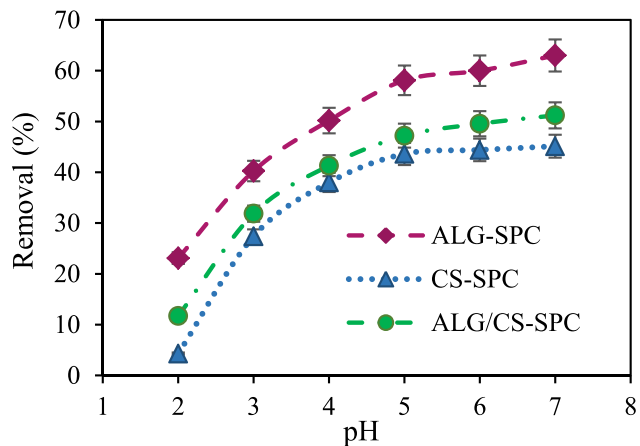

Fig. 6. Effect of biopolymer for granulation of SPC on adsorption of Ni(II) at different solution pH values.

capacity of 11.07 mg/g, which is closer to the actual equilibrium adsorption capacity of 11 mg/g, while the pseudo-first order model predicts a value of 9.821 mg/g.

The diffusion models used in this study are based on approximations of the mass transfer steps controlling the adsorption process. The film diffusion model and the Crank intraparticle model (for long contact times: $q/q_e > 0.3$) were chosen from among the diffusion models, and their nonlinear forms are presented in Table 3. Boyd's external diffusion model indicates that the external mass transfer resistance is directly proportional to the effective liquid film diffusion coefficient and inversely proportional to the equilibrium constant of adsorption (Wang and Guo, 2020). On the other hand, the Crank model neglects the external film resistance, and the equation is an exact solution for the
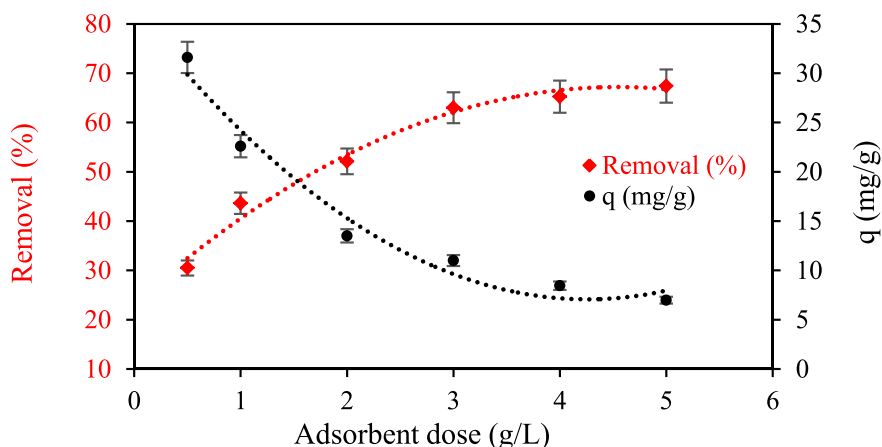
Fig. 7. Effect of ALG-SPC dosage on adsorption of Ni(II) (C0 = 50 mg/L, and pH = 7).
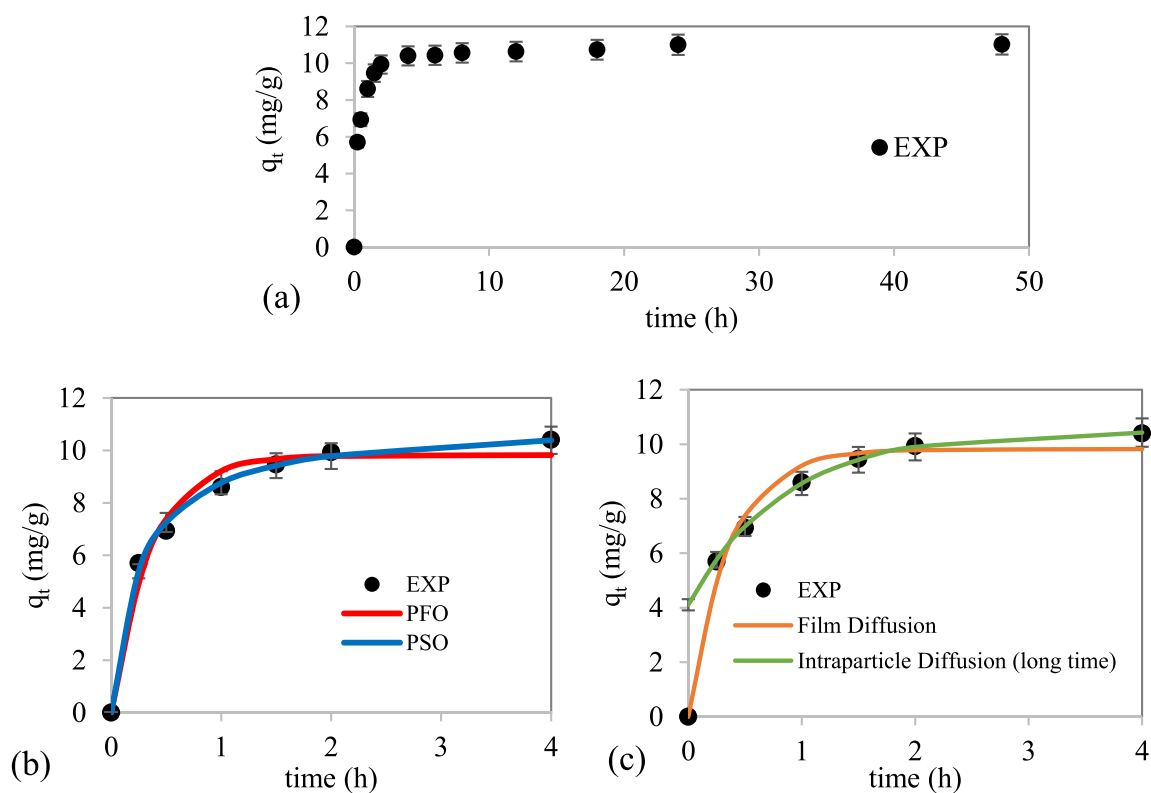

Fig. 8. (a) Kinetic experimental data for Ni(II) adsorption onto ALG-SPC, (b) reaction-based kinetic models and (c) diffusion-based kinetic models to explain the experimental data.

homogeneous surface diffusion model (HSDM) (Crank, 1979).

The statistical analysis indicated that the intraparticle diffusion model provided a better fit to the kinetic data than the film diffusion model. This suggests that the intraparticle diffusion step is the key factor in the adsorption of Ni(II) onto ALG-SPC, rather than external film diffusion. This may be due to the fact that ALG-SPC has a granular shape, that results in a large internal surface area enclosed by alginate, and is less accessible to external species compared to a powdered sorbent. Therefore, despite the external mass transfer resistance resulting from the boundary layer thickness around the particles, intraparticle diffusion was found to play a more significant role. This is because the process was modelled for the entire adsorption period before equilibrium, not just for the first few minutes of contact, where film diffusion is the better fitting

model. The surface diffusion coefficient for Ni(II) on ALG-SPC was calculated to be 2.44×10^{-11} m²/s, assuming an average particle radius of 0.85 mm for the adsorbent beads.

Several appropriate isotherm models, such as Langmuir, Freundlich, Sips, and Dubinin-Radushkevich models, were used to study and model the adsorption behaviour of the adsorbent ALG-SPC at equilibrium. While the Langmuir model is one of the simplest and oldest, it remains the most flexible model for describing monolayer adsorption on homogeneous surfaces of adsorbents. The Freundlich model, on the other hand, is a classical model usually applicable for adsorption of solutes from a dilute aqueous solution. Table 4 and Fig. 9(a) demonstrate the relatively good fit of the Langmuir model and the better fit of the Freundlich model to explain the equilibrium adsorption data. The results

Table 3

(a) Kinetic experimental data and equilibrium time and (b) reaction-based kinetic models for the data at the initial hours of contact before equilibrium.

Kinetic models		Equations/parameters[a]	Ni adsorption onto ALG-SPC	
			Statistical analysis	Parameters
Reaction-based models	Pseudo-first order model	$q_t = q_e\left(1 - e^{-k_1 t}\right)$	$R^2 = 0.9799$ SSE = 1.582 RMSE = 0.5625	$q_e = 9.821$ (mg/g) $k_1 = 2.781$ (1/h) $h_1 = k_1 q_e = 27.3122$ (mg/g.h)
	Pseudo-second order model	$q_t = \dfrac{k_2 q_e^2 t}{1 + k_2 q_e t}$	$R^2 = 0.9968$ SSE = 0.2488 RMSE = 0.2231	$q_e = 11.07$ (mg/g) $k_2 = 0.3434$ (g/mg.h) $h_2 = k_2 q_e^2 = 42.0819$ (mg/g.h)
Diffusional models	Boyd's external (film) diffusion model	$q_t = q_e\left(1 - \exp(-R_f t)\right)$ $R_f = \dfrac{3D_e}{R\Delta r_0 K}$	$R^2 = 0.9799$ SSE = 1.582 RMSE = 0.5625	$q_e = 9.821$ (mg/g) $R_f = 2.781$ (1/h)
	Crank intraparticle model	(For long contact time, $\frac{q_t}{q_e} > 0.3$) $q_t = q_e\left(1 - \dfrac{6}{\pi^2}\exp\left(\dfrac{-D_s\pi^2 t}{R^2}\right)\right)$	$R^2 = 0.9994$ SSE = 0.01062 RMSE = 0.05153	$q_e = 10.48$ (mg/g) $D_s\pi^2/R^2 = 1.2$ (1/h) $D_s = 2.44 \times 10^{-11}$ (m²/s)

[a] t (h): time, q_e and q_t (mg/g): the equilibrium and time-dependent adsorption capacities, k_1 (1/h): pseudo-first order kinetic constant, k_2 (g/mg.h): pseudo-second order kinetic constant, h (mg/g.h): initial sorption rate, R_f (1/h): liquid film external resistance, D_e (m²/h): effective liquid film diffusion coefficient, R (m): radius of adsorbent beads, Δr_0 (m): the thickness of liquid film surrounding the adsorbent particle, K: equilibrium constant of adsorption, D_s (m²/h): intraparticle surface diffusion coefficient.

indicate that Ni(II) cations on ALG-SPC are mainly adsorbed through multilayer adsorption. The strong adsorption isotherm is indicated by the value of $1/n_F$, which is less than 0.7 and serves as the exponent of nonlinearity.

In this study, the monolayer adsorption capacity of ALG-SPC was determined to be 21.10 mg/g, and this value was compared with the corresponding values reported in the literature for clay-based adsorbents (Table 5). The table also includes the conditions used to measure these monolayer adsorption capacities.

Although the Freundlich model is useful in providing information on the heterogeneity of the adsorbent surface and the exponential distribution of active site energies, it cannot predict the saturation of the adsorbent surface by the adsorbate (Naiya et al., 2009). To estimate the maximum adsorption capacity that can be adsorbed by ALG-SPC, a combination of the Langmuir and Freundlich models (Sips model) was investigated. This 3-parameter isotherm model yielded better agreement with the experimental equilibrium data and allowed for an estimation of the maximum adsorption capacity about 52.776 mg/g.

The Dubinin-Radushkevich (D-R) model is an additional model that can be utilized to estimate the nature of adsorption mathematically, based on the average free energy (E) and the degree of infinite surface coverage (Fig. 9(b)). The linear form of this model can be found in Table 4, along with the parameters obtained by linear fitting of the experimental data. The maximum theoretical saturation capacity estimated by the D-R model is 53.44 mg/g, and the mean free energy of sorption is 15.07 kJ/mol. The magnitude of this energy, which falls within the range of 8–16 kJ/mol, supports the role of physical sorption and ion exchange (Pan et al., 2020) in the adsorption of Ni(II) by

Table 4

The isotherm models for describing Ni(II) adsorption experimental data.

Isotherm models	Equations/parameters[a]	Ni adsorption onto ALG-SPC	
		Statistical analysis	Parameters
Langmuir	$q_e = \dfrac{q_{mL}K_L C_e}{1 + K_L C_e}$	$R^2 = 0.9631$ SSE = 13.65 RMSE = 1.508	$q_{mL} = 21.10$ (mg/g) $K_L = 0.0548$ (L/mg)
Freundlich	$q_e = K_F C_e^{\frac{1}{n_F}}$	$R^2 = 0.9959$ SSE = 1.523 RMSE = 0.5038	$K_F = 4.942$ (mg/g)(mg/L)$^{-1/nF}$ $n_F = 3.8595$
Sips	$q_e = \dfrac{q_{ms}K_s C_e^{\frac{1}{n_s}}}{1 + K_s C_e^{\frac{1}{n_s}}}$	$R^2 = 0.9971$ SSE = 1.085 RMSE = 0.4658	$q_{ms} = 52.776$ (mg/g) $K_s = 0.0854$ (mg/L)$^{-1/ns}$ $n_s = 2.741$
Dubinin-Radushkevich	$\ln q_e = \ln q_{mD} - B\varepsilon^2$ $\varepsilon = RT\ln\left(1 + \dfrac{1}{C_e}\right)$ $E = 1/\sqrt{2B}$	$R^2 = 0.9882$ SSE = 0.011 RMSE = 0.0463	$q_m = 53.44$ (mg/g) $E = 15.07$ (kJ/mol)

[a] C_e (mg/L): the solute concentration at equilibrium (in D-R model: g/g), q_e (mg/g): Equilibrium adsorption capacity, q_{mL}(mg/g): Langmuir maximum monolayer adsorption capacity, K_L (L/mg), K_F (mg/g)(mg/L)$^{-1/nF}$, and K_s (mg/L)$^{-1/ns}$: Langmuir, Freundlich, and Sips constants, n_F and n_s: dimensionless exponents of Freundlich and Sips models, q_{ms} (mg/g): Sips model maximum adsorption capacity, q_{mD} (mg/g): theoretical monolayer saturation capacity of D-R model, B (mol/kJ)²: D-R model constant, ϵ (kJ/mol): Polanyi potential, R (kJ/mol.K): Gas constant, T (K): Absolute temperature, E (kJ/mol): mean energy of sorption.

ALG-SPC.

Fig. 10 displays the FTIR spectra of both the fresh ALG-SPC and the Ni(II)-saturated sorbent. Although many of the peaks in both spectra are identical, including Al−O, Si−O, and Si−O−Si, there is a noticeable difference in the FTIR spectrum of ALG-SPC after adsorption of Ni(II) regarding the ion-water interaction, which is evident in the OH-stretching at 3430 cm^{-1} (Kitadai et al., 2014). Furthermore, the FTIR spectrum of the Ni-adsorbed sample reveals a peak at 610 cm^{-1} that can be assigned to the Ni−O stretching band. This peak, often observed as a sharp band, is typically reported as confirmation of the formation of NiO nanoparticles (Sharma et al., 2015). The Ni−O−H bending vibration, which usually occurs at 580 cm^{-1} (Budipramana et al., 2014), may lead to a slight change in the FTIR spectrum of ALG-SPC saturated with Ni due to the low adsorbed concentration.

3.3. Competitive adsorption

To evaluate the efficacy of ALG-SPC in removing Ni(II) in the presence of another metal ion (Cr(VI)), and to determine the selectivity of the adsorbent, a range of adsorption experiments were conducted at various pH values using solutions containing both species. The findings are presented in Fig. 11. The chart does not display the percentage removal of Cr(VI) by adsorption from solutions that contain only one contaminant since it was insignificant.

Fig. 11 indicates that the presence of Cr(VI) in the solution does not significantly affect the adsorption of Ni(II) across a wide pH range. The graph also displays the pH$_{pzc}$ of ALG-SPC, which was measured to be 5.4 using the pH drift method. At pH levels lower than pH$_{pzc}$, the surface of ALG-SPC is relatively positive, while at higher pH values, the surface of the adsorbent becomes negative. Throughout the investigated pH range, Ni existed in the form of Ni^{2+}. However, some studies have reported the possibility of Ni(II) precipitation as Ni(OH)$_2$ at a pH above 6.5 (Vieira et al., 2010). In this study, precipitation was observed at a pH higher
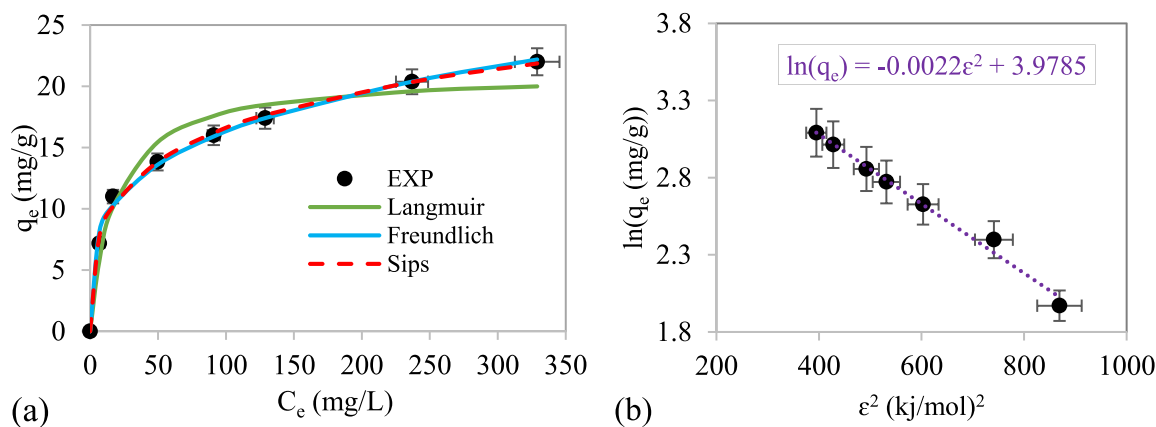
Fig. 9. The adsorption isotherm experimental data fitted to the non-linear forms of Langmuir, Freundlich and Sips models and (b) the linear form of Dubinin-Radushkevich model.

Table 5
Comparison of monolayer Ni(II) adsorption capacity of ALG-SPC with other clay-based adsorbents reported in literature.

| Adsorbent	Initial concentration (mg/L)	pH	Adsorbent dosage (g/L)	Monolayer Ni(II) adsorption capacity (mg/g)	Ref.
Montmorillonite	10–50	5.7	2	21.14	Gupta and Bhattacharyya (2006)
Poly(hydroxyzirconium) modified montmorillonite				10.45	
TBA-derivative montmorillonite				8.50	
Kaolinite				7.05	
Poly(hydroxyzirconium) modified kaolinite				4.05	
TBA-derivative kaolinite				2.75	
Montmorillonite	10–50	5.7	2	28.4	Bhattacharyya and Gupta (2008b)
Acid-activated montmorillonite				29.5	
Kaolinite				10.4	
Acid-activated kaolinite				11.9	
Ball-milled natural clay	10–90	7	2	29.76	Maleki and Karimi-Jashni (2017)
Kaolinite	10–50	5.7	2	10.4	Bhattacharyya and Gupta (2008a)
ZrO-kaolinite				8.8	
Montmorillonite				28.4	
ZrO-montmorillonite				22.0	
Alginate-encapsulated silica pillared clay	30–400	7	3	21.10	This work
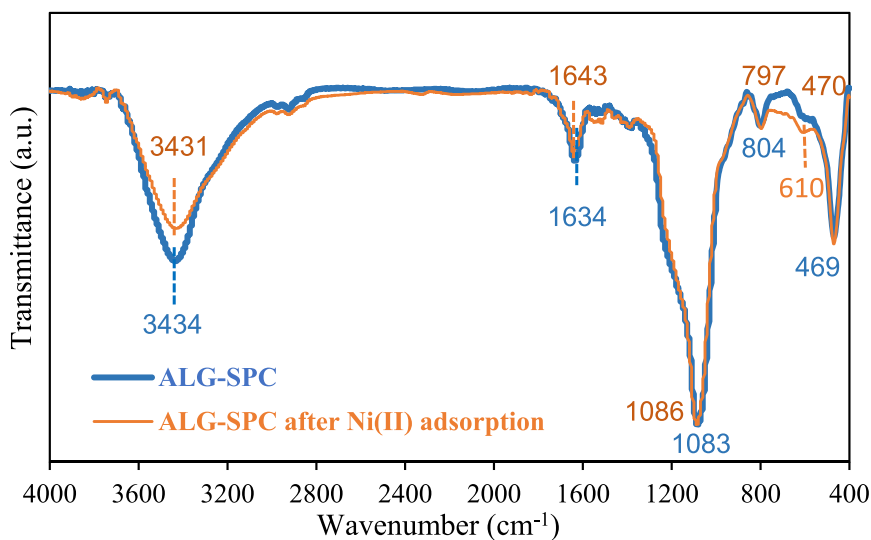
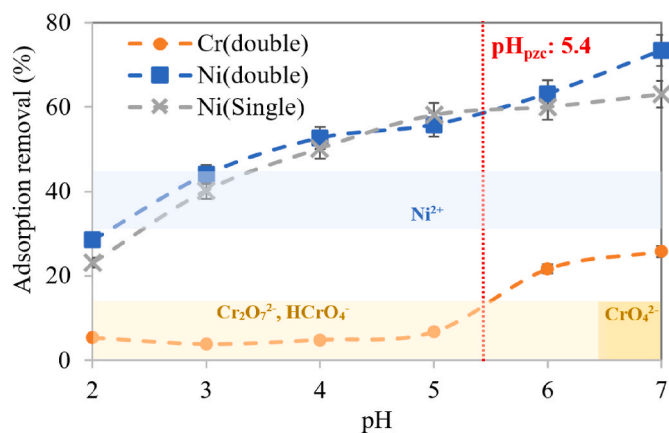**Fig. 10.** FTIR spectra of ALG-SPC before and after adsorption of Ni(II) from aqueous solution.

Fig. 11. Effect of Cr(VI) anions on Ni(II) adsorption from binary contaminated solutions by ALG-SPC.

than 7 via blank tests.

As mentioned previously, the adsorption of Ni^{2+} is favoured due to the speciation of Ni(II) and the surface charge of the adsorbent at a pH higher than pH_{pzc}, resulting in an increasing trend of adsorption capacity. This is further enhanced by the competition of H^+ cations at highly acidic pH values. Nevertheless, it is evident that the adsorption capacity of Ni^{2+} is not negligible at lower pH values, implying that electrostatic adsorption is just one of the mechanisms involved in Ni^{2+} adsorption. Conversely, Ni^{2+} adsorption is more effective at pH values above pH_{pzc} due to the negative surface charge of ALG-SPC and the involvement of electrostatic attraction. The adsorption of a significant number of Ni^{2+} cations on the adsorbent's surface may lead to an affinity for the anionic Cr(VI) species present in the solution (Maamoun et al., 2022). The speciation of Cr(VI) in aqueous solution at different pH values is as follows: $Cr_2O_7^{2-}$ and $HCrO_4^-$ at pH < 6.5 and CrO_4^{2-} at higher pH values (Szabó et al., 2018). In turn, these adsorbed anionic species can enhance Ni^{2+} cations' adsorption; thus, the Ni(II) adsorption removal at high pH from binary solutions is more efficient than that from single pollutant solutions. Consequently, the adsorbent (ALG-SPC) is selective for Ni at pH values below pH_{pzc} and does not adsorb chromium. Furthermore, Cr(VI) has no significant effect on Ni adsorption;

however, Ni(II) adsorption may promote the adsorption of Cr(VI) anions by Ni^{2+} adsorbed species.

3.4. Desorption and cyclic performance

In the final step, the percentage of Ni(II) desorption from the saturated ALG-SPC sorbent was investigated using different solvents, including acidic solutions (HCl and HNO$_3$, 0.1 M), electrolyte solutions (KCl and NaCl, 0.1 M), and pure methanol. The obtained desorption percentages are depicted in Fig. 12(a), with the highest desorption percentage observed for acidic solutions. As the pH decreases under acidic conditions and H^+ cations accumulate in the solutions, the positive surface charge of the adsorbent leads to an increased competition between H^+ and Ni^{2+}. Consequently, the electrostatic repulsion between the Ni(II) cation and the positively charged adsorbent surface reduces the adsorption capacity.

The desorption rates obtained for the electrolytes NaCl and KCl were lower (about 45%) than those for the acidic solutions, and a significant weight loss of the adsorbent occurred during the desorption experiments. These results suggest that exposure to these electrolytes can degrade the structure of the adsorbent, making them unsuitable for Ni (II) desorption. Typically, these solutions are useful solvents for desorbing species adsorbed through an ion exchange mechanism. In contrast, methanol exhibited negligible ability to desorb the adsorbed Ni.

As HCl showed the best performance in Ni desorption, the Ni-saturated sorbent was recovered using this solution and used in the second adsorption experiment for Ni adsorption. These adsorption-desorption cycles were repeated three times sequentially. The results in Fig. 12(b) indicate that the ALG-SPC sorbent can be efficiently recovered for Ni adsorption with negligible loss in adsorption efficiency and weight.

4. Conclusion

Granulated modified silica pillared clays were produced from Iranian local clay by encapsulating it with biopolymers, alginate, chitosan, or a combination of both. The characterization experiments (FESEM, XRD, XRF, BET, and FTIR) confirmed the successful conversion of SPC powder to granulated modified SPCs and showing the changes in the porous,
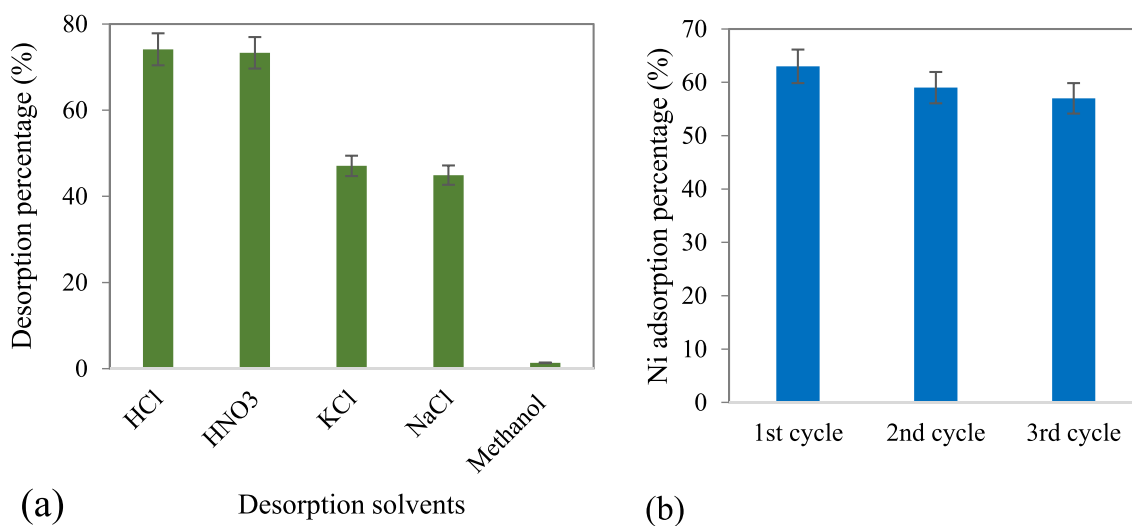

Fig. 12. (a) Ni recovery by different solvents from saturated ALG-SPC (adsorption conditions: initial concentration: 50 mg/L, dosage: 3 g/L, pH: 7, at room temperature, for 24 h; desorption conditions: 5 g adsorbent/L solvents including aqueous solution of HCl, HNO$_3$, KCl, NaCl 0.1 M, pure methanol, room temperature, 24 h), (b) the cyclic performance of ALG-SPC regenerated with HCl (0.1 M) in three adsorption-desorption.

chemical, and crystalline phases of SPC. Chitosan had a significant negative role on the porosity of modified clay, with CS-SPC showing a very small S_{BET} and a relatively non-porous structure. Batch adsorption experiments were conducted to remove Ni(II) from aqueous solutions using different types of granular SPCs. The granular sorbents were found to be easier and more practical to apply, separate, and recover. The results showed that ALG-SPC had better performance than ALG/CS-SPC, with the former having appropriate strong electrostatic attraction between the negatively charged alginate and Ni(II) cations. The worst performance was observed with CS-SPC, which had the weakest chemical groups and S_{BET}. The mixed sample (ALG/CS-SPC) showed medium performance, but closer to ALG-SPC. pH effect experiments and FTIR characterization were conducted to better understand the functional groups involved and adsorption mechanism. Kinetic and equilibrium adsorption experiments were performed to estimate the best kinetic models and the main mass transfer steps involved in Ni(II) adsorption. The Langmuir monolayer adsorption capacity of the most effective sample (ALG-SPC) was found to be 20.10 mg/g, comparable to the values reported for the adsorption capacity of other types of clay sorbents towards Ni(II). ALG-SPC showed negligible affinity for Cr(VI) in single-component solutions; however, in binary solutions, especially at pH > pH_{pzc}, the electrostatic attraction between Cr(VI) and Ni(II) led to the adsorption of Cr(VI) as the adsorbed Ni(II) increased. Therefore, the selectivity of the sorbent in the presence of Ni(II) and Cr(VI) was investigated, and it was found that ALG-SPC had the best performance for Ni(II), especially at acidic pH. The recovery of adsorbed Ni from saturated ALG-SPC was carried out using the elution method. The best performance (desorption percentage >70%) was obtained with acidic solutions (0.1 M HCl or HNO3). However, electrolyte solutions of NaCl and/or KCl with desorption percentages of about 45%, which destroyed the structure of the adsorbent beads, were not promising. To conclude, the study examined the conversion of SPC powder to granulated modified forms using three different mixtures, and evaluated the performance of encapsulated SPC for Ni and Cr(VI) adsorption in single and binary systems, which had not been done before.

Declaration of competing interest

The authors declare that they have no known competing financial interests or personal relationships that could have appeared to influence the work reported in this paper.

Data availability

Data will be made available on request.

References

Addy, M., Losey, B., Mohseni, R., Zlotnikov, E., Vasiliev, A., 2012. Adsorption of heavy metal ions on mesoporous silica-modified montmorillonite containing a grafted chelate ligand. Appl. Clay Sci. 59, 115–120. https://doi.org/10.1016/j.clay.2012.02.012.

Aziz, S.B., Abdulwahid, R.T., Rasheed, M.A., Abdullah, O.G., Ahmed, H.M., 2017. Polymer blending as a novel approach for tuning the SPR peaks of silver nanoparticles. Polymers 9, 486. https://doi.org/10.3390/polym9100486.

Balcı, S., Tomul, F., 2023. Catalytic wet peroxide oxidation of phenol through mesoporous silica-pillared clays supported iron and/or titanium incorporated catalysts. J. Environ. Manag. 326, 116835 https://doi.org/10.1016/j.jenvman.2022.116835.

Bhattacharyya, K.G., Gupta, S.S., 2008a. Adsorption of Fe (III), Co (II) and Ni (II) on ZrO–kaolinite and ZrO–montmorillonite surfaces in aqueous medium. Colloids Surf. A. Physicochem. Eng. Asp. 317, 71–79. https://doi.org/10.1016/j.colsurfa.2007.09.037.

Bhattacharyya, K.G., Gupta, S.S., 2008b. Uptake of Ni (II) ions from aqueous solution by kaolinite and montmorillonite: influence of acid activation of the clays. Separ. Sci. Technol. 43, 3221–3250. https://doi.org/10.1080/01496390802219638.

Budipramana, Y., Ersam, T., Kurniawan, F., 2014. Synthesis nickel hydroxide by electrolysis at high voltage. ARPN J. Eng. Appl. Sci. ISSN: 1819-6608 9, 2074–2077.

Çeçen, F., Aktas, Ö., 2011. Activated Carbon for Water and Wastewater Treatment: Integration of Adsorption and Biological Treatment. John Wiley & Sons, Weinheim.

Chitraprabha, K., Sathyavathi, S., 2018. Phytoextraction of chromium from electroplating effluent by Tagetes erecta (L.). Sustain. Environ. Res. 28, 128–134. https://doi.org/10.1016/j.serj.2018.01.002.

Crank, J., 1979. The Mathematics of Diffusion, second ed. Oxford university press, London.

Daemi, H., Barikani, M., 2012. Synthesis and characterization of calcium alginate nanoparticles, sodium homopolymannuronate salt and its calcium nanoparticles. Sci. Iran 19, 2023–2028. https://doi.org/10.1016/j.scient.2012.10.005.

Dincer, B.Y., Balcı, S., Tomul, F., 2020. In-situ mesoporous silica pillared clay synthesis and effect of titanium and iron incorporation to structural properties. Microporous Mesoporous Mater. 305, 110342 https://doi.org/10.1016/j.micromeso.2020.110342.

Farajfaed, S., Sharifian, S., Asasian-Kolur, N., Sillanpää, M., 2021. Granular silica pillared clay for levofloxacin and gemifloxacin adsorption from aqueous systems. J. Environ. Chem. Eng. 9, 106306 https://doi.org/10.1016/j.jece.2021.106306.

Golnaraghi Ghomi, A., Asasian-Kolur, N., Sharifian, S., Golnaraghi, A., 2020. Biosorption for sustainable recovery of precious metals from wastewater. J. Environ. Chem. Eng. 8, 103996 https://doi.org/10.1016/j.jece.2020.103996.

Gupta, S.S., Bhattacharyya, K.G., 2006. Adsorption of Ni (II) on clays. J. Colloid Interface Sci. 295, 21–32. https://doi.org/10.1016/j.jcis.2005.07.073.

Han, Y.-S., Lee, S.-H., Choi, K.H., in Park, 2010. Preparation and characterization of chitosan–clay nanocomposites with antimicrobial activity. J. Phys. Chem. Solid. 71, 464–467. https://doi.org/10.1016/j.jpcs.2009.12.012.

Ince, M., Ince, O.K., 2019. Heavy metal removal techniques using response surface methodology: water/wastewater treatment. In: Biochemical Toxicology-Heavy Metals and Nanomaterials. IntechOpen. https://doi.org/10.5772/intechopen.88915.

Jaishankar, M., Tseten, T., Anbalagan, N., Mathew, B.B., Beeregowda, K.N., 2014. Toxicity, mechanism and health effects of some heavy metals. Interdiscipl. Toxicol. 7, 60. https://doi.org/10.2478/intox-2014-0009.

Kitadai, N., Sawai, T., Tonoue, R., Nakashima, S., Katsura, M., Fukushi, K., 2014. Effects of ions on the OH stretching band of water as revealed by ATR-IR spectroscopy. J. Solut. Chem. 43, 1055–1077. https://doi.org/10.1007/s10953-014-0193-0.

Maamoun, I., Bensaida, K., Eljamal, R., Falyouna, O., Tanaka, K., Tosco, T., Sugihara, Y., Eljamal, O., 2022. Rapid and efficient chromium (VI) removal from aqueous solutions using nickel hydroxide nanoplates (nNiHs). J. Mol. Liq. 358, 119216 https://doi.org/10.1016/j.molliq.2022.119216.

Maleki, S., Karimi-Jashni, A., 2017. Effect of ball milling process on the structure of local clay and its adsorption performance for Ni (II) removal. Appl. Clay Sci. 137, 213–224. https://doi.org/10.1016/j.clay.2016.12.008.

Mao, H., Zhu, K., Li, B., Yao, C., Kong, Y., 2014. Synthesis of titania modified silica-pillared clay (SPC) with highly ordered interlayered mesoporous structure for removing toxic metal ion Cr (VI) from aqueous state. Appl. Surf. Sci. 292, 1009–1019. https://doi.org/10.1016/j.apsusc.2013.12.113.

Mnasri-Ghnimi, S., Frini-Srasra, N., 2019. Removal of heavy metals from aqueous solutions by adsorption using single and mixed pillared clays. Appl. Clay Sci. 179, 105151 https://doi.org/10.1016/j.clay.2019.105151.

Naiya, T.K., Chowdhury, P., Bhattacharya, A.K., Das, S.K., 2009. Saw dust and neem bark as low-cost natural biosorbent for adsorptive removal of Zn (II) and Cd (II) ions from aqueous solutions. Chem. Eng. J. 148, 68–79. https://doi.org/10.1016/j.cej.2008.08.002.

Najafi, H., Asasian-Kolur, N., Sharifian, S., 2021a. Adsorption of chromium (VI) and crystal violet onto granular biopolymer-silica pillared clay composites from aqueous solutions. J. Mol. Liq. 344, 117822 https://doi.org/10.1016/j.molliq.2021.117822.

Najafi, H., Asasian-Kolur, N., Sharifian, S., Haddadi, B., Jordan, C., Harasek, M., 2022a. Calcium alginate encapsulated pillared clay beads for adsorption of Ni (Ii) from aqueous solution. Chem. Eng. Trans. 94, 1213–1218. https://doi.org/10.3303/CET2294202.

Najafi, H., Farajfaed, S., Zolgharnian, S., Mirak, S.H.M., Asasian-Kolur, N., Sharifian, S., 2021b. A comprehensive study on modified-pillared clays as an adsorbent in wastewater treatment processes. Process Saf. Environ. Protect. 147, 8–36. https://doi.org/10.1016/j.psep.2020.09.028.

Najafi, H., Mohammadi, S.A., Asasian-Kolur, N., Sharifian, S., 2022b. Adsorptive removal of gemifloxacin from aqueous solution using mesoporous Fe-incorporated silica pillared clay followed by thermal regeneration. Mater. Today Commun., 104932 https://doi.org/10.1016/j.mtcomm.2022.104932.

Noh, J.S., Schwarz, J.A., 1989. Estimation of the point of zero charge of simple oxides by mass titration. J. Colloid Interface Sci. 130, 157–164. https://doi.org/10.1016/0021-9797(89)90086-6.

Pan, S.-Y., Syu, W.-J., Chang, T.-K., Lee, C.-H., 2020. A multiple model approach for evaluating the performance of time-lapse capsules in trapping heavy metals from water bodies. RSC Adv. 10, 16490–16501. https://doi.org/10.1039/D0RA03017A.

Patel, H., 2021. Review on solvent desorption study from exhausted adsorbent. J. Saudi Chem. Soc. 25, 101302 https://doi.org/10.1016/j.jscs.2021.101302.

Pfeifer, A., Skerget, M., 2020. A review: a comparison of different adsorbents for removal of Cr (VI), Cd (II) and Ni (II). Turk. J. Chem. 44, 859–883. https://doi.org/10.3906/kim-2002-21.

Revathi, M., Kavitha, B., Vasudevan, T., 2005. Removal of nickel ions from industrial plating effluents using activated alumina as adsorbent. J. Environ. Health Sci. Eng. 47, 1–6. https://doi.org/10.1016/j.clay.2019.105151.

Roca Jalil, M.E., Toschi, F., Baschini, M., Sapag, K., 2018. Silica pillared montmorillonites as possible adsorbents of antibiotics from water media. Appl. Sci. 8, 1403. https://doi.org/10.3390/app8081403.

Sahoo, T.R., Prelot, B., 2020. Adsorption processes for the removal of contaminants from wastewater: the perspective role of nanomaterials and nanotechnology. In: Nanomaterials for the Detection and Removal of Wastewater Pollutants. Elsevier, pp. 161–222. https://doi.org/10.1016/C2018-0-02642-0.

Sayın, S., Depci, T., Naz, M., Sezer, S., Karaaslan, M.G., Aras, A., Uğur, S., Çetin, Z., Saygılı, E.İ., Ateş, B., 2022. Characterization and evaluation of the antimicrobial properties of algal alginate; a potential natural protective for cosmetics. J. Pharm. Res. 26, 198–209. https://doi.org/10.29228/jrp.117.

Sharma, A.K., Desnavi, S., Dixit, C., Varshney, U., Sharma, A., 2015. Extraction of nickel nanoparticles from electroplating waste and their application in production of bio-diesel from biowaste. Int. J. Chem. Eng. Appl. 6, 156. https://doi.org/10.7763/IJCEA.2015.V6.472.

Szabó, M., Kalmár, J., Ditrói, T., Bellér, G., Lente, G., Simic, N., Fábián, I., 2018. Equilibria and kinetics of chromium (VI) speciation in aqueous solution–a comprehensive study from pH 2 to 11. Inorg. Chim. Acta. 472, 295–301. https://doi.org/10.1016/j.ica.2017.05.038.

Varma, R., Vasudevan, S., 2020. Extraction, characterization, and antimicrobial activity of chitosan from horse mussel modiolus modiolus. ACS Omega 5, 20224–20230. https://doi.org/10.1021/acsomega.0c01903.

Vieira, M.G., Neto, A.A., Gimenes, M.L., Da Silva, M.G., 2010. Sorption kinetics and equilibrium for the removal of nickel ions from aqueous phase on calcined Bofe bentonite clay. J. Hazard Mater. 177, 362–371. https://doi.org/10.1016/j.jhazmat.2009.12.040.

Wang, J., Guo, X., 2020. Adsorption kinetic models: physical meanings, applications, and solving methods. J. Hazard Mater. 390, 122156 https://doi.org/10.1016/j.jhazmat.2020.122156.

Wardani, A.K., Hakim, A.N., Khoiruddin, Destifen, W., Goenawan, A., Wenten, I.G., 2017. Study on the influence of applied voltage and feed concentration on the performance of electrodeionization in nickel recovery from electroplating wastewater. In: AIP Conference Proceedings. AIP Publishing LLC, p. 30004.

World Health Organization, 2021. A Global Overview of National Regulations and Standards for Drinking-Water Quality, 92400236.

Wu, X., Xia, X., Chen, Y., Lu, Y., 2016. Mesoporous Al-incorporated silica-pillared clay interlayer materials for catalytic hydroxyalkylation of phenol to bisphenol F. RSC Adv. 6, 74028–74038. https://doi.org/10.1039/C6RA15161B.

Yang, S., Liang, G., Gu, A., Mao, H., 2013. Synthesis of mesoporous iron-incorporated silica-pillared clay and catalytic performance for phenol hydroxylation. Appl. Surf. Sci. 285, 721–726. https://doi.org/10.1016/j.apsusc.2013.08.116.